Thermal generation of droplet soliton in chiral magnet

Vladyslav M. Kuchkin,[1,2,*] Pavel F. Bessarab,[3,4,5] and Nikolai S. Kiselev[1]

[1]*Peter Grünberg Institute and Institute for Advanced Simulation, Forschungszentrum Jülich and JARA, 52425 Jülich, Germany*

[2]*Department of Physics, RWTH Aachen University, 52056 Aachen, Germany*

[3]*Science Institute of the University of Iceland, 107 Reykjavík, Iceland*

[4]*Department of Physics and Engineering, ITMO University, 197101 St. Petersburg, Russia*

[5]*School of Science and Technology, Örebro University, Fakultetsgatan 1, 70281 Örebro, Sweden*

(Received 19 November 2021; revised 21 April 2022; accepted 21 April 2022; published 2 May 2022)

Controlled creation of localized magnetic textures beyond conventional π-skyrmions is an important problem in the field of magnetism. Here, by means of spin dynamics simulations, Monte Carlo simulations, and harmonic transition state theory we demonstrate that an elementary chiral magnetic soliton with zero topological charge—the chiral droplet—can be created by thermal fluctuations in the presence of the tilted magnetic field. The proposed protocol relies on an unusual kinetics combining the effects of the entropic stabilization and low-energy barrier for the nucleation of a topologically trivial state. Following this protocol by varying temperature and the tilt of the external magnetic field, one can selectively generate chiral droplets or π-skyrmions in a single system. The coexistence of two distinct magnetic solitons establishes a basis for a rich magnetization dynamics and opens up the possibility for the construction of more complex magnetic textures such as skyrmion bags and skyrmions with chiral kinks.

DOI: 10.1103/PhysRevB.105.184403

I. INTRODUCTION

The model of chiral magnets allows surprisingly many spatially localized statically stable solutions. Together with the originally reported solutions, also known as $k\pi$-skyrmions (Sks) [1], a large variety of nonaxially symmetric solitons with an arbitrary topological index were recently discovered in the two-dimensional (2D) model of a chiral magnet. The latter include skyrmion bags [2,3] and Sks with chiral kinks (CKs) [4–7]. Recently, the direct observation of skyrmion bags by means of Lorentz transmission electron microscopy and their current-induced motion were reported in Ref. [8]. The experimental evidence for CKs was provided in Ref. [9]. The coexistence of various types of solitons in a single system is fundamentally interesting and technologically appealing. However, since the localized states beyond conventional Sks are typically metastable states, their controllable nucleation is challenging.

Here we suggest a protocol for generating an elementary magnetic soliton containing a single CK—the chiral droplet (CD), also referred to as a chimera skyrmion [10]—by means of thermal fluctuations and oblique magnetic field. Figure 1 shows the magnetic vector fields for a π-skyrmion [Fig. 1(a)] and the CD [Fig. 1(c)]. The invariant which defines the topological charge is

$$Q = \frac{1}{4\pi}\int \mathbf{n}\cdot(\partial_x\mathbf{n}\times\partial_y\mathbf{n})dxdy. \tag{1}$$

For a π-skyrmion, $Q=-1$, and for a CD, $Q=0$. We refer to the CD as an elementary chiral soliton because it is the most compact nonaxially symmetric soliton containing only one CK. The CD texture was previously reported as a statically stable solution [5,10] and a transient state during the asymmetric Sk collapse [11–13]. In contrast to $k\pi$-skyrmions, the interparticle interaction potentials for a CD with other solitons are strongly asymmetric due to the presence of the CK [4]. As a consequence, CDs may attract or repel other solitons depending on their mutual orientation. This provides a basis for skyrmion fusion and, thereby, the creation of more complex magnetic textures.

Although CDs represent excitations in the ferromagnetic (FM) background, their large entropy enables entropic stabilization, similar to what was reported for conventional π-skyrmions [14–16]. On the other hand, CDs belong to a class of topologically trivial solitons [5]. Because of that one may expect lower energy barriers for their nucleation compared to that for topologically nontrivial textures. As a result, there are prerequisites for effective thermal generation of CDs. Indeed, we found that under a tilted magnetic field and moderate thermal fluctuations, the spontaneous nucleation of CDs dominates the π-Sk nucleation by several orders of magnitude. It is noteworthy that by varying the temperature and the tilt angle of the external field one can selectively nucleate either π-Sks or CDs. These findings are supported by the consistence of stochastic Landau-Lifshitz-Gilbert (LLG) simulations, Monte Carlo simulations, and analysis based on the transition state theory.

*v.kuchkin@fz-juelich.de

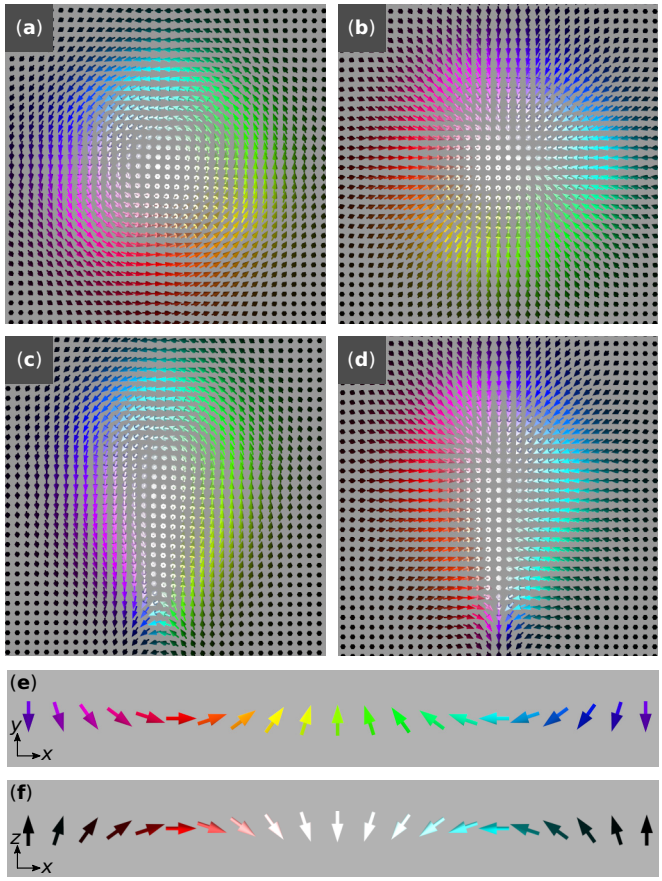

FIG. 1. (a) and (b) show the π-skyrmion stabilized with Bloch and Neel types of DMI, respectively. (c) and (d) show the chiral droplets stabilized with Bloch and Neel types of DMI, respectively. The CD is calculated at $h = 0.65$ and $u = 0$. The magnetic textures in (b) and (d) can be obtained from the textures in (a) and (c) by rotating all spins by 90° counterclockwise about the z axis. (e) and (f) illustrate the standard color code used for visualization of the magnetization vector field. (e) shows vectors lying in the xy-plane ($n_z = 0$), and (f) shows vectors in the xz-plane ($n_y = 0$).

II. MODEL

We consider a classical spin Hamiltonian on a square lattice:

$$E = -J\sum_{\langle i,j\rangle}\mathbf{n}_i\cdot\mathbf{n}_j - \sum_{\langle i,j\rangle}\mathbf{D}_{ij}\cdot[\mathbf{n}_i\times\mathbf{n}_j] - \mu_s\mathbf{B}\sum_i\mathbf{n}_i, \quad (2)$$

were $\mathbf{n}_i$ is the normalized magnetization vector at lattice site i; J and $\mathbf{D} = D\hat{\mathbf{r}}_{ij}$ are the Heisenberg exchange constant and Dzyaloshinskii-Moriya vector, respectively; $\hat{\mathbf{r}}_{ij}$ is the unit vector between sites i and j; μ_s is the magnitude of the magnetic moment at each site; and $\mathbf{B}$ is the external magnetic field. The symbol $\langle i, j\rangle$ denotes summation over unique nearest-neighbor pairs. The ratio between J and D defines the equilibrium period of helical spin spirals, $L_D = 2\pi Ja/D$, with a being the lattice constant, and characteristic magnetic field, $B_D = D^2/(J\mu_s)$.

All simulations were performed for the Dzyaloshinskii-Moriya interaction (DMI) of the Bloch type, which is commonly attributed to the bulk crystals of chiral magnets. However, the particular choice of DMI does not affect the main results and modifies only the chirality of magnetic textures. A comparison of magnetic textures for a CD in the cases of Bloch and Neel types of DMI is shown in Figs. 1(c) and 1(d), respectively.

We consider the case where magnetic field is tilted with respect to the plane normal, $\mathbf{h} = \mathbf{B}/B_D = h(\sin\vartheta\cos\varphi, \sin\vartheta\sin\varphi, \cos\vartheta)$, and parametrized by the polar angle ϑ and azimuthal angle φ. For parameters J and D in our simulations and providing a relatively large $L_D = 64a$, the Hamiltonian (2) becomes nearly isotropic in the xy-plane. In this case, the choice of angle φ does not affect the results, but for definiteness we fix $\varphi = -\pi/4$.

We simulate spin dynamics at finite temperature using the stochastic LLG equation:

$$\frac{\partial\mathbf{n}_i}{\partial t} = -\mathbf{n}_i\times\left(\mathbf{B}^i_{\text{eff}} + \mathbf{B}^i_{\text{fluc}}\right) + \alpha\mathbf{n}_i\times\frac{\partial\mathbf{n}_i}{\partial t}, \quad (3)$$

where t is a dimensionless time scaled by $J\gamma\mu_s^{-1}$, with γ being the gyromagnetic ratio; α is the Gilbert damping parameter; $\mathbf{B}^i_{\text{eff}} = -\frac{1}{J}\frac{\partial E}{\partial\mathbf{n}_i}$ is a dimensionless effective field; and $\mathbf{B}^i_{\text{fluc}}$ is the fluctuating field representing uncorrelated Gaussian white noise with the correlation coefficient proportional to temperature T. For the numerical integration of Eq. (3), we use the semi-implicit method provided in Ref. [17] assuming $\alpha = 0.3$ and time step $\Delta t = 0.01$. For the chosen coupling parameters we estimate the critical temperature, $T_c \simeq 0.7J/k_B$ (see Ref. [18]). For the results presented below, the temperature is always $T < T_c$ and given in units of J/k_B.

III. RESULTS

A. Stochastic LLG simulations

The top row of images in Fig. 2 provides representative snapshots of the LLG simulations showing the system at various temperatures and different tilt angles of the external magnetic field, $\vartheta = 0$ in Fig. 2(a) and $\vartheta = 0.4$ in Fig. 2(b). To make the presence of the localized magnetic textures in the system more evident, in the bottom row of images we provide corresponding snapshots of the system after cooling by setting $T = 0$ in (3). In the case of perpendicular magnetic field, $\vartheta = 0$, we observe spontaneous nucleation of only π-Sks, while at tilted magnetic field, $\vartheta = 0.4$, we observe the nucleation of CDs. Noticeably, the temperature required for the nucleation of CD is significantly lower than that for the π-Sk nucleation [compare the snapshots in Figs. 2(a) and 2(b) at $T = 0.18\,J/k_B$]. Thus, applying the tilted field and varying the temperature, one can selectively nucleate either CDs or π-Sks. At high temperature, however, in both cases, we observe the emergence of π-Sks, which in an appropriate field range tend to form a regular lattice. For the tilted field and intermediate temperatures, on the other hand, the isolated solitons exhibit an additional degree of freedom. As seen in Fig. 2(b) for $T = 0.3$, they tend to elongate and can transform into the spiral state. In contrast, a close-packed π-Sk lattice remains stable up to a critical tilt angle, $\vartheta_c \approx 50°$ [19].

The CD orientation in 2D space can be defined by the in-plane component of the net magnetization of the CD, $\mathbf{m} = \sum_i(\mathbf{n}_i - \mathbf{n}_0)$, where $\mathbf{n}_0$ is the magnetization far from the soliton $\mathbf{n}_0 = \mathbf{n}(\mathbf{r})$, for $r \to \infty$. In the presence of a tilted magnetic

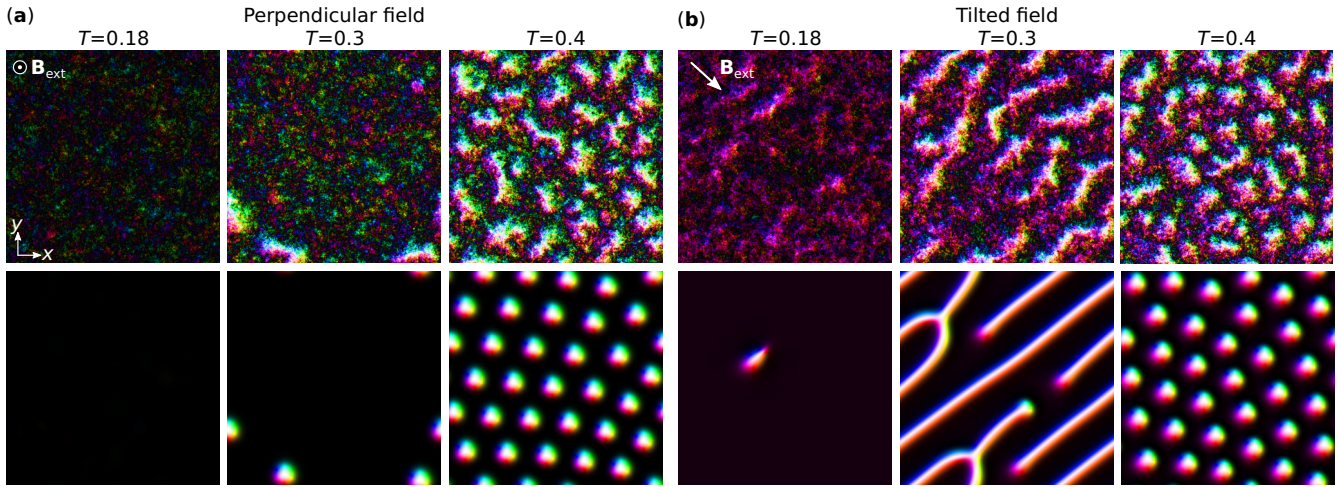

FIG. 2. (a) illustrates the case of perpendicular magnetic field, $h = 0.643$, $\vartheta = 0$ and (b) corresponds to the tilted magnetic field, $h = 0.645$, $\vartheta = 0.4$. The simulations were performed on a square domain, $L_x = L_y = 8L_D$, with periodic boundary conditions in the xy-plane, and $\mathbf{n}(\mathbf{r})||\mathbf{B}_{ext}$ in the initial state. The top row of images represents the snapshots of the system at different temperatures taken at thermal equilibrium after $\sim 10^6$ LLG iterations. Each image in the bottom row corresponds to the top image after setting $T = 0$ and energy relaxation. The color code is identical to that shown in Fig. 1(e) and 1(f).

field, vector **m** of the CD is always parallel to the in-plane projection of the external field, **h**.

Figure 3 illustrates the details of the CD nucleation process, as obtained from the LLG simulations. The black curve in Fig. 3(a) shows an averaged out-of-plane component of magnetization, $\mathcal{N} = \sum_i n_{i,z}/N$, where i runs over all N spins. With time, $\mathcal{N}$ converges to its equilibrium value, which for the chosen parameters equals 0.74. The Monte Carlo (MC) simulations [18] are fully consistent with the results of LLG simulations and show a similar behavior of $\mathcal{N}$ in reaching thermal equilibrium.

π-Sks are characterized by topological charge $Q = -1$; hence, the event of their nucleation can be identified by calculating Q. In contrast, the CDs have zero topological charge, which makes this approach inapplicable. To identify the presence of CDs in the system we employ an alternative method based on time tracing of the net magnetization, as described in the following. We split the whole simulated domain into overlapping subdomains Ω_j of fixed size $L_D \times L_D$ containing $N' = L_D^2/a^2$ spins. Taking into account these periodic boundary conditions, the total number of such subdomains equals the number of spins in the system N. At each time step, we calculate the averaged out-of-plane magnetization for each subdomain, $\mathcal{N}_j = \sum_i n_{i,z}/N'$, $i \in \Omega_j$. Then, we identify the subdomain Ω_m with minimal $\mathcal{N}_j$, denoted $\mathcal{N}_m$. The red curve in Fig. 3(a) shows the representative dependency of $\mathcal{N}_m$ on

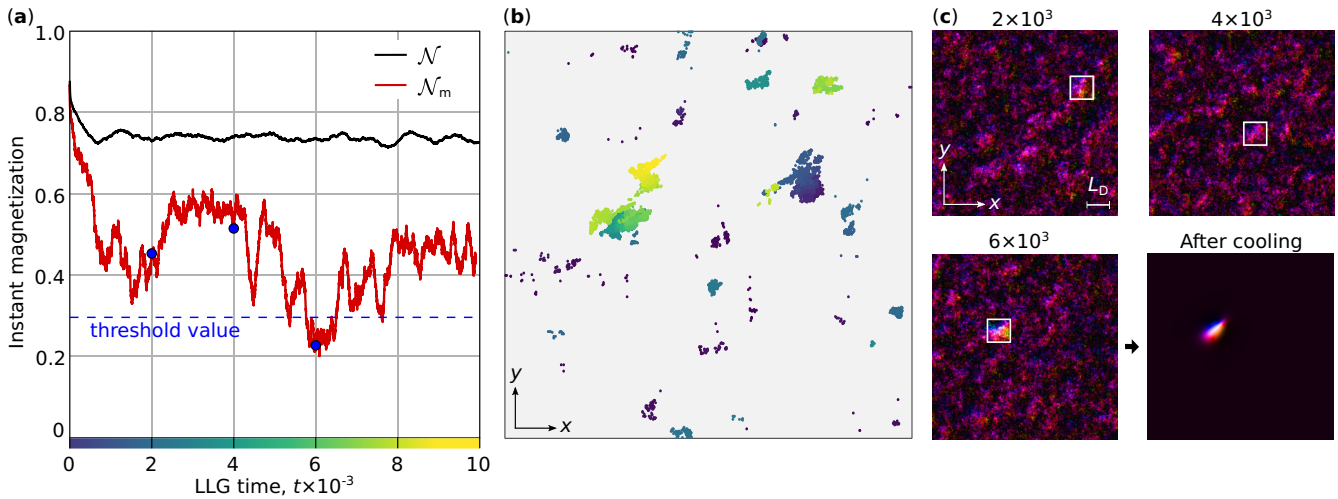

FIG. 3. (a) shows the evolution of the average magnetization $\mathcal{N}$ (black) and its maximal value $\mathcal{N}_m$ (red) at temperature $T = 0.18$, as obtained in the LLG simulations. The dashed blue line corresponds to the threshold value of 0.3 for $\mathcal{N}_m$. The position of subdomain Ω_m corresponding to $\mathcal{N}_m$ is given in (b); the colors encode the time [see the color bar in (a)]. Blue dots in (a) mark instants of time for which magnetic textures are shown in (c). The white squares of size $L_D \times L_D$ correspond to the subdomains Ω_m. The right bottom image in (c) is obtained after relaxation at $T = 0$.

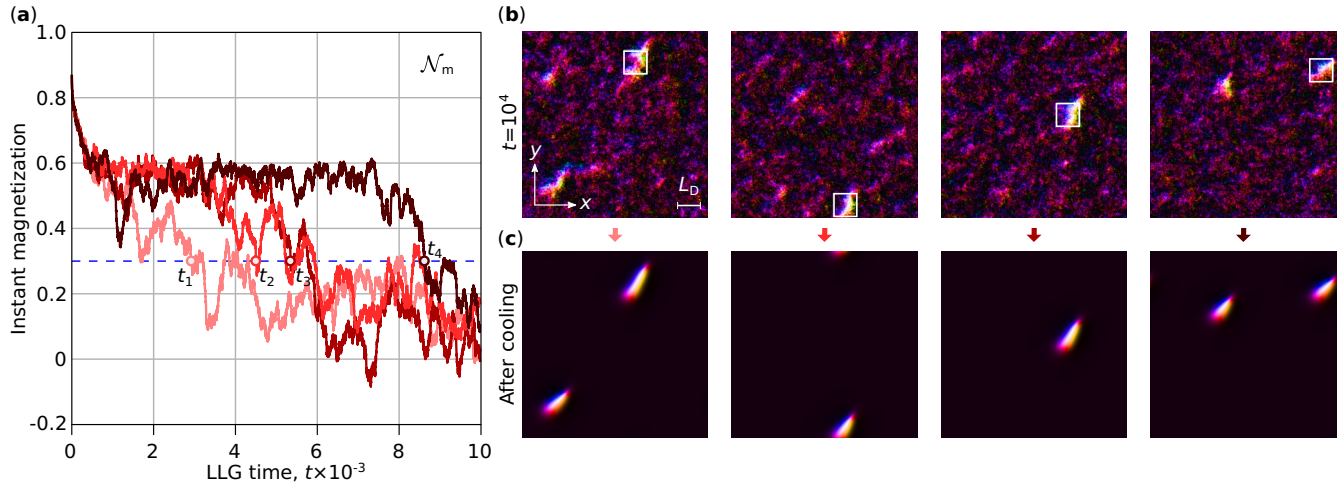

FIG. 4. (a) shows the minimal value of the average magnetization $\mathcal{N}_m$ as a function of time for 4 of 10 LLG simulations giving rise to CD nucleation within a time window of 10^4. The times at which $\mathcal{N}_m$ drops below the threshold value of 0.3 are $t_1 = 2.93$, $t_2 = 4.51$, $t_3 = 5.40$, and $t_4 = 8.64$. (b) shows the final states at $t = 10^4$ for each of four independent LLG simulations, and (c) shows the same states after cooling at $T = 0$.

the LLG simulation step. The event of soliton nucleation is signaled by a drop in $\mathcal{N}_m$ below an empirically estimated threshold value and is then confirmed by abrupt cooling [see the corresponding images in Fig. 3(c)]. The expected position of the soliton is given by the coordinates of the Ω_m, as depicted in Fig. 3(b). The CD nucleation is well reproduced in MC simulations [18].

To estimate the average time required for CD nucleation we performed 10 independent LLG simulations for a time window of $t = 10^4$ (10^6 LLG iterations) at identical conditions, $T = 0.18Jk_B^{-1}$, and $\vartheta = 0.4$ rad. In 4 of 10 simulations, we observe a drop in $\mathcal{N}_m$ below the threshold value and nucleation of the CDs. The $\mathcal{N}_m(t)$ dependences for these four successful runs are presented in Fig. 4(a) together with snapshots of the system at the final stage of the simulations at $t = 10^4$ [Fig. 4(b)] and after the relaxation [Fig. 4(c)]. The six LLG simulations that did not show CD nucleation within that time window are not presented. The average time for CD nucleation can be estimated as $\langle t\rangle = \nu \sum t_i = 8.59 \times 10^3$, where $\nu = 4/10$ is the number of successful nucleation events over the total number of LLG simulations, and t_i ($i = 1, 2, 3, 4$) are the values of time at which $\mathcal{N}_m(t)$ crosses the threshold value [see the open circles in Fig. 4(a)]. The transition rate $k = 1/\langle t\rangle$ for CD nucleation is $\sim 10^{-4}$.

To estimate the real-time scale at which the above process occurs, one should take realistic values of the Heisenberg exchange constant and magnetic moment. For instance, for $J = 5$ meV and $\mu_s = \mu_B$ the whole time interval in Fig. 3(a) corresponds to $\sim$3.3 ns, which represents a typical timescale at which LLG simulations can be carried out reliably [20]. At lower temperatures, the simulation of the nucleation process of the CD might require a time window above hundreds of nanoseconds, which is extremely time-consuming [21].

Figure 5(a) illustrates the stability range of the CD in terms of the absolute value of the applied magnetic field $h = |\mathbf{h}|$ and the tilt angle ϑ for $T = 0$. The CD stability domain is confined between the critical lines defined by the collapse field $h_c(\vartheta)$ and by the stretching (or elliptical) instability field $h_s(\vartheta)$: $h_s(\vartheta) < h < h_c(\vartheta)$. The range of h where CD is stable shrinks with increasing ϑ, and at $\vartheta \simeq 1.1$ the CD becomes unstable. Remarkably, the critical field h_s coincides with the phase transition line between the skyrmion lattice and spin spiral states. Therefore, the CD always represents a metastable solution while the lowest-energy state in that range of fields is the skyrmion lattice. Nevertheless, at moderate temperatures, the nucleation of the CDs dominates over the nucleation of energetically more favorable π-Sks. At elevated temperatures, we observe the transition into the skyrmion lattice within an accessible simulation time irrespective of the field tilt angle (see Fig. 2 at $T = 0.4$).

B. Harmonic transition state theory calculations

Further understanding of thermal nucleation of the CD states can be obtained using the harmonic transition state theory (HTST) [22,23]. Within the HTST, the rate of transition between states X and Y is described by Arrhenius's law,

$$k^{X\to Y} = \nu^{X\to Y} \exp\left(-\frac{\Delta E^{X\to Y}}{k_B T}\right), \tag{4}$$

where the energy barrier $\Delta E^{X\to Y}$ can be identified from the minimum energy path (MEP) connecting X and Y as the energy difference between the highest point along the MEP—the first-order saddle point (SP) on the energy surface of the system—and the minimum at X. The pre-exponential factor $\nu^{X\to Y}$ incorporating the dynamical and entropic contributions to the transition rate is defined by the curvature of the energy surface at the minimum and at the SP [16]. Note that HTST assumes no barrier recrossings by the dynamical trajectories; therefore, the HTST-predicted rates typically provide a qualitative picture of the transition kinetics. Precise values of the rates can be obtained by calculating the recrossing correction [24,25], but this goes beyond the scope of the present study.

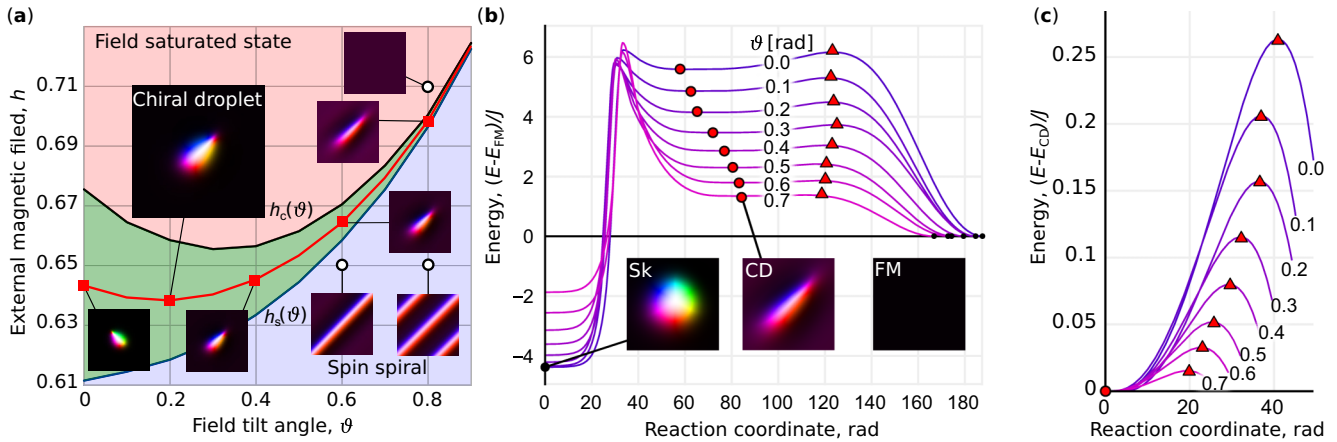

FIG. 5. Stability diagram of CD in terms of the magnetic field h and its tilt ϑ. For $h < h_s$ (blue region), the CD becomes unstable with respect to stretching. For $h > h_c$ (red region), the CD collapses to FM. The red line corresponds to the intermediate values of the stability range in terms of h; magnetic textures of CDs for some points on this curve are shown in the insets. (b) shows the energy variation along the MEPs connecting the Sk, CD, and FM states for different parameters h, ϑ along the red line in (a). Red circles denote the energy minima corresponding to CD; red triangles mark the saddle points between the CD and FM states. (c) shows a zoom of (b), with the zero of energy defined at the CD state.

The MEP calculations using the geodesic nudged elastic band method [26,27] show that direct nucleation of the Sk state from the FM background is possible only for $\vartheta \lesssim 0.1$. For larger tilts of the external field, the MEP for the Sk nucleation and annihilation passes through an intermediate energy minimum corresponding to the CD state [see Fig. 5(b)]. Therefore, the system initially prepared in the FM state undergoes a transition to the CD state before it may reach the Sk state, which is also observed in the spin dynamics and Monte Carlo simulations [18]. As seen from Fig. 5(b), the energy barrier between the FM state and CD state gradually decreases with ϑ. This explains the enhancement in the CD generation as the tilt of the field increases. On the other hand, the energy of the saddle point between the CD and π-Sk states depends weakly on the tilt angle. It is mostly defined by the discretization of the system. Approaching the micromagnetic regime with increasing L_D, the energy barrier $\Delta E^{\mathrm{FM}\to\mathrm{Sk}}$ increases [28], which makes the π-Sk nucleation less probable.

Another important aspect of the problem is that the energy of the CD is always higher than that of the π-Sk. That makes a big difference in other magnetic systems allowing the coexistence of topological and nontopological solitons. For instance, in perpendicular anisotropy films, a magnetic bubble with topological index $Q = -1$ may undergo the transition into a topologically trivial state with $Q = 0$. In the literature, this effect induced by the tilted external field is known as the transition between type-I and type-II bubbles [29]. Modern high-resolution Lorentz transmission electron microscopy provides an observation of this effect in detail (see, e.g., Refs. [30,31]). This type of transition in bubble domain materials has a high probability because, above a specific critical tilt angle, the energy of a topologically trivial type-II bubble becomes lower than the energy of a normal type-I bubble [31]. As we noted above, that is not the case for 2D chiral magnets where the π-Sk is the lowest energy state at any tilt angle, $0 \leqslant \vartheta \leqslant \frac{1}{2}\pi$. Because of that, the transition from the π-Sk to the CD represents an unlikely event.

The CD energy minimum appears to be quite shallow [Fig. 5(b)], suggesting a quick collapse of the CD state. However, the HTST calculations, in agreement with the spin dynamics simulations, predict the opposite. The rates of transitions involving the CD state (FM $\rightleftarrows$ CD, CD $\rightleftarrows$ Sk) are characterized by very different values of the energy barrier and pre-exponential factor, as can be seen from the Arrhenius plots shown in Fig. 6. In particular, the pre-exponential factor $\nu^{\mathrm{FM}\to\mathrm{CD}}$ for the FM $\to$ CD transition—the nucleation of CDs—is much larger than that for the backward transition. Despite the very low energy barrier for the CD $\to$ FM transition, the nucleation of CDs becomes more intensive than their annihilation in the FM state above a certain crossover temperature. For small tilts of the external field, the CD

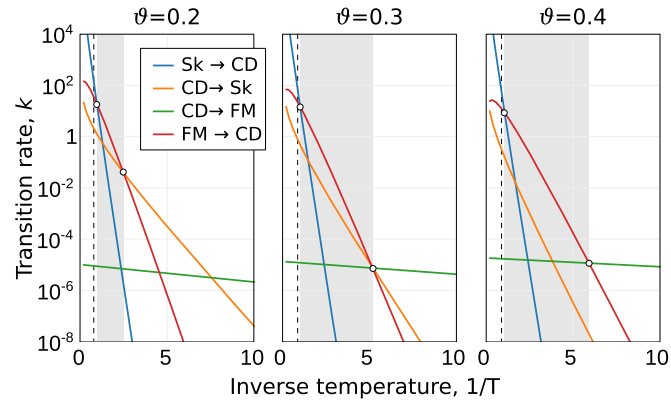

FIG. 6. Rates of various magnetic transitions (as indicated in the legend) as a function of the inverse thermal energy for various tilts ϑ of the magnetic field. The amplitude of h corresponds to the middle line of the CD stability range in Fig. 5(a). The gray regions mark the temperature range with the maximal intensity of the FM $\to$ CD transition. The vertical dashed line corresponds to the Curie temperature $1/T_c$. The transition rate k is provided in units of inverse unitless time t, the same as in our LLG simulations.

quickly transits into the Sk state. However, with increasing ϑ the CD $\rightarrow$ Sk transition is progressively suppressed due to the increasing energy barrier $\Delta E^{\mathrm{CD}\rightarrow\mathrm{Sk}}$ [see Fig. 5(b)]. The temperature range where the CD nucleation dominates the annihilation by several orders of magnitude increases with ϑ (see the gray domain in Fig. 6). The HTST calculations therefore provide a consistent interpretation of the thermally induced creation of CDs observed in our spin dynamics and MC simulations. In particular, for $\vartheta = 0.4$ and $T = 0.18Jk_{\mathrm{B}}^{-1}$ $(1/T = 5.56)$ the transition rate k for CD nucleation has the same order of magnitude, $\sim 10^{-4}$, as the one we estimated from LLG simulations.

IV. CONCLUSIONS

In conclusion, we proposed a protocol for the creation of CDs by means of thermal fluctuations in a 2D chiral magnet under a tilted magnetic field. The protocol takes advantage of the entropic stabilization and relatively low energy barrier for the nucleation of a topologically trivial magnetic soliton. By varying the temperature and the tilt of the applied field, CDs and Sks can be generated selectively in a single system. Coexisting CDs and Sks can further be used as building blocks for creating more complex magnetic solitons in chiral systems.

ACKNOWLEDGMENTS

The authors would like to thank T. Sigurjónsdóttir and F. Rybakov for helpful discussions. This work was funded by Deutsche Forschungsgemeinschaft (DFG) through SPP 2137 "Skyrmionics" Grant No. KI 2078/1-1, the Russian Science Foundation (Grant No. 19-72-10138), the Icelandic Research Fund (Grants No. 184949 and No. 217750), the University of Iceland Research Fund (Grant No. 15673), and the Swedish Research Council (Grant No. 2020-05110).

[1] A. Bogdanov and A. Hubert, J. Magn. Magn. Mater. **195**, 182 (1999).
[2] F. N. Rybakov and N. S. Kiselev, Phys. Rev. B **99**, 064437 (2019).
[3] D. Foster, C. Kind, P. J. Ackerman, J.-S. B. Tai, M. R. Dennis, and I. I. Smalyukh, Nat. Phys. **15**, 655 (2019).
[4] V. M. Kuchkin and N. S. Kiselev, Phys. Rev. B **101**, 064408 (2020).
[5] V. M. Kuchkin, B. Barton-Singer, F. N. Rybakov, S. Blügel, B. J. Schroers, and N. S. Kiselev, Phys. Rev. B **102**, 144422 (2020).
[6] V. M. Kuchkin, K. Chichay, B. Barton-Singer, F. N. Rybakov, S. Blügel, B. J. Schroers, and N. S. Kiselev, Phys. Rev. B **104**, 165116 (2021).
[7] R. Cheng, M. Li, A. Sapkota, A. Rai, A. Pokhrel, T. Mewes, C. Mewes, D. Xiao, M. De Graef, and V. Sokalski, Phys. Rev. B **99**, 184412 (2019).
[8] J. Tang, Y. Wu, W. Wang, L. Kong, B. Lv, W. Wei, J. Zang, M. Tian, and H. Du, Nat. Nanotechnol. **16**, 1086 (2021).
[9] M. Li, A. Sapkota, A. Rai, A. Pokhrel, T. Mewes, C. Mewes, D. Xiao, M. De Graef, and V. Sokalski, J. Appl. Phys. **130**, 153903 (2021).
[10] L. Rózsa, K. Palotás, A. Deák, E. Simon, R. Yanes, L. Udvardi, L. Szunyogh, and U. Nowak, Phys. Rev. B **95**, 094423 (2017).
[11] L. Desplat, J.-V. Kim, and R. L. Stamps, Phys. Rev. B **99**, 174409 (2019).
[12] F. Muckel, S. von Malottki, C. Holl, B. Pestka, M. Pratzer, P. F. Bessarab, S. Heinze, and M. Morgenstern, Nat. Phys. **17**, 395 (2021).
[13] S. Meyer, M. Perini, S. von Malottki, A. Kubetzka, R. Wiesendanger, K. von Bergmann, and S. Heinze, Nat. Commun. **10**, 3823 (2019).
[14] L. Desplat, D. Suess, J.-V. Kim, and R. L. Stamps, Phys. Rev. B **98**, 134407 (2018).
[15] S. von Malottki, P. F. Bessarab, S. Haldar, A. Delin, and S. Heinze, Phys. Rev. B **99**, 060409(R) (2019).
[16] A. S. Varentcova, S. von Malottki, M. N. Potkina, G. Kwiatkowski, S. Heinze, and P. F. Bessarab, npj Comput. Mater. **6**, 193 (2020).
[17] J. H. Mentink, M. V. Tretyakov, A. Fasolino, M. I. Katsnelson and Th. Rasing, J. Phys.: Condens. Matter **22**, 176001 (2010).
[18] See Supplemental Material at http://link.aps.org/supplemental/10.1103/PhysRevB.105.184403 for the details of the Monte Carlo simulations and the estimation for the Curie temperature.
[19] A. O. Leonov and I. Kézsmárki, Phys. Rev. B **96**, 214413 (2017).
[20] R. D. McMichael, M. J. Donahue, and D. G. Porter, and J. Eicke, J. Appl. Phys. **89**, 7603 (2001).
[21] L. Lopez-Diaz, D. Aurelio, L. Torres, E. Martinez, M. A. Hernandez-Lopez, J. Gomez, O. Alejos, M. Carpentieri, G. Finocchio, and G. Consolo, J. Phys. D **45**, 323001 (2012).
[22] P. F. Bessarab, V. M. Uzdin, and H. Jónsson, Phys. Rev. B **85**, 184409 (2012).
[23] P. F. Bessarab, V. M. Uzdin, and H. Jónsson, Z. Phys. Chem. **227**, 1543 (2013).
[24] J. C. Keck, Adv. Chem. Phys. **13**, 85 (1967).
[25] A. F. Voter and J. D. Doll, J. Chem. Phys. **82**, 80 (1985).
[26] P. F. Bessarab, V. M. Uzdin, and H. Jónsson, Comput. Phys. Commun. **196**, 335 (2015).
[27] P. F. Bessarab, Phys. Rev. B **95**, 136401 (2017).
[28] B. Heil, A. Rosch, and J. Masell, Phys. Rev. B **100**, 134424 (2019).
[29] A. P. Malozemoff and J. C. Slonczewski, *Magnetic Domain Walls in Bubble Materials* (Academic, New York, 1979).
[30] X. Yu, M. Mostovoy, Y. Tokunaga, W. Zhang, K. Kimoto, Y. Matsui, Y. Kaneko, N. Nagaosa, and Y. Tokura, Proc. Natl. Acad. Sci. USA **109**, 8856 (2012).
[31] Y. Wu, J. Tang, B. Lyu, L. Kong, Y. Wang, J. Li, Y. Soh, Y. Xiong, M. Tian, and H. Du, Appl. Phys. Lett. **119**, 012402 (2021).